Published in final edited form as:
Clin Cancer Res. 2010 March 1; 16(5): 1542–1552. doi:10.1158/1078-0432.CCR-08-1812.

Evaluation of Treatment Associated Inflammatory Response on Diffusion Weighted-MRI and FDG-PET Imaging Biomarkers

Craig J. Galbán[1,2], **Mahaveer S Bhojani**[1,4], **Kuei C. Lee**[1,2], **Charles R. Meyer**[1,2], **Marcian Van Dort**[1,2], **Kyle Kuszpit**[1,2], **Robert A. Koeppe**[2], **Rajesh Ranga**[4], **Bradford A. Moffat**[1,2], **Timothy D. Johnson**[5], **Thomas L. Chenevert**[1,2], **Alnawaz Rehemtulla**[1,2,4], and **Brian D. Ross**[1,2,3]

[1] Center for Molecular Imaging, University of Michigan, School of Medicine, Ann Arbor, Michigan

[2] Department of Radiology, University of Michigan, School of Medicine, Ann Arbor, Michigan

[3] Department of Biological Chemistry, University of Michigan, School of Medicine, Ann Arbor, Michigan

[4] Department of Radiation Oncology, University of Michigan, School of Medicine, Ann Arbor, Michigan

[5] Department of Biostatistics, University of Michigan, School of Medicine, Ann Arbor, Michigan

Abstract

Purpose—Functional imaging biomarkers of cancer treatment response offer the potential for early determination of outcome through assessment of biochemical, physiological, and micro-environmental readouts. Cell death may result in an immunological response thus complicating interpretation of biomarker readouts. This study evaluated the temporal impact of treatment-associated inflammatory activity on diffusion-MRI and FDG-PET imaging biomarkers to delineate the effects of the inflammatory response on imaging readouts.

Experimental Design—Rats with intracerebral 9L gliosarcomas were separated into four groups consisting of control, an immunosuppressive agent dexamethasone (Dex), 1,3-bis(2-chloroethyl)-1-nitrosourea (BCNU), and BCNU+Dex (BCNU+Dex). Animals were imaged using diffusion-weighted MRI and FDG-PET at 0, 3 and 7 days post-treatment.

Results—In the BCNU and BCNU+Dex treated animal groups, diffusion values increased progressively over the 7 day study period to about 23% over baseline. FDG %SUV decreased at day 3 (−30.9%) but increased over baseline levels at day 7 (+20.1%). FDG-PET of BCNU+Dex treated animals were found to have %SUV reductions of −31.4% and −24.7% at days 3 and 7, respectively following treatment. Activated macrophages were observed on day 7 in the BCNU treatment group with much fewer found in the BCNU+Dex group.

Conclusions—Results revealed treatment-associated inflammatory response following tumor therapy resulted in accentuation of tumor diffusion response along with a corresponding increase in tumor FDG uptake due to the presence of glucose-consuming activated macrophages. The dynamics and magnitude of potential inflammatory response should be considered when interpreting imaging biomarker results.

Requests for reprints: Brian D. Ross, Ph.D., The University of Michigan, Center for Molecular Imaging, Department of Radiology, 109 Zina Pitcher Place, Biomedical Sciences Research Building, Ann Arbor, MI 48109-0220, Phone: 734-763-2099, Fax: 734-763-5447 bdross@umich.edu.

Disclosure: TLC, BDR and AR have a financial interest in the underlying diffusion technology presented in this manuscript.

Keywords

Diffusion; MRI; ADC; positron emission tomography; FDG; brain tumor

INTRODUCTION

Promising approaches for individualization of oncology patient care include development of imaging-based biomarkers as early readouts of therapeutic efficacy (1,2). Imaging readouts can be based upon a pre-treatment measured parameter or a parameter that is found to change early on following treatment initiation. Molecular imaging biomarkers under active evaluation for early treatment assessment include diffusion magnetic resonance imaging (3-6) and 2-[^{18}F]-fluoro-2-deoxy-D-glucose-positron emission tomography (FDG-PET) (7-16).

Diffusion-weighted MRI (DW-MRI) can be used to quantify the Brownian motion of water molecules within tumor tissue and is expressed as an apparent diffusion coefficient (ADC). The random motion of water molecules is influenced by the underlying tumor morphology (i.e. cellular density) (17,18), therefore it is sensitive to early changes in tumor cell death during successful treatment regimes. More specifically, as the tumor cells are killed during treatment, diffusion values have been shown to increase in those regions of positive response, thus providing an opportunity for the use of DW-MRI determined changes in ADC as a surrogate for cellular death. Because the removal of tumor macromolecular debris takes time for the overall tumor mass to shrink, changes in tumor diffusion is considered to be an early event in the successful treatment of a tumor thereby allowing for early and noninvasive imaging of treatment response within an individual patient. Data supporting the application of DW-MRI for cancer treatment response monitoring was initially reported in the 9L glioma model (19) and has since been supported by numerous studies using a variety of tumor models (20-34) and in cancer patients (3,35-46). Moreover, treatment-induced changes in ADC values of brain tumors have been shown to be dose-dependent in animal models (21,29) and predictive of outcome in brain tumor patients (47).

FDG-PET is a nuclear imaging-based biomarker which is under active evaluation in part as an early cancer treatment response indicator. This approach uses a radiotracer, [18F]-FDG, for detection of treatment efficacy as alterations in tumor glucose uptake following treatment are anticipated due to tumor cell death. The standard uptake values (SUV's) of FDG-PET have been shown to be sensitive to early changes in gliomas following treatment (7,48-50). A decrease in tumor FDG uptake using scintillation counting on excised tumors following radiotherapy was reported in mouse mammary carcinomas and a rat hepatoma (48). More recently, several reports have shown that chemotherapy (10,49,51) and radiotherapy (13,51, 52) results in early increases in FDG uptake of brain tumors in humans. This contradiction has yet to be adequately explained.

Diffusion MRI and FDG-PET imaging biomarkers have been identified to be sensitive to early changes in the tumor micro-environment following cytotoxic intervention, thus it is important to understand the relationship/correlation of these two biomarkers for assessing treatment response. Moreover, since tumor inflammatory response can occur following treatment and since [18F]-FDG cannot differentiate tumor from inflammation (53), it would be prudent to investigate the relative sensitivities of each approach to inflammation. To our knowledge there have been no studies investigating the relationship between diffusion MRI and FDG-PET simultaneously in an experimental tumor model undergoing therapy. In this study, longitudinal diffusion MRI and FDG-PET images of the 9L orthotopic glioma model during chemotherapy (+/− immunosuppressive therapy) was accomplished allowing for the quantification of temporal changes for each biomarker and evaluation of the relative influence of the tumor

inflammatory response, namely macrophage infiltration and activation, on the individual imaging biomarker readouts.

MATERIALS AND METHODS

Intracranial Tumor Implantation

The rat 9L gliosarcoma cell line (University of California, San Francisco, CA) was cultured as a monolayer in Dulbecco's modified Eagle's medium with glutamine, supplemented with 10% inactivated fetal calf serum in incubator at 37°C with 5% CO_2 and 95% air. Cells were harvested and re-suspended in serum-free media at the time of tumor implantation.

All animal work was carried out in the animal facility at University of Michigan in accordance with federal, local, and institutional guidelines. Male Fischer 344 rats (Charles River Breeding Laboratories, Wilmington, MA) weighing between 125 and 150g were used for cell implantation. Animals were anesthetized using a xylazine (13 mg/kg)/ketamine (87 mg/kg) mixture dosed i.p. A small skin incision was made over the right hemisphere and a 1 mm diameter burr hole was made through the skull using a high speed drill. The 9L cell suspension was prepared to consist of a suspension of 1×10^5 cells in 5μl serum-free medium, which was introduced through a 27-gauge needle into the depth of 2.5 mm. Following implantation the site was cleaned and the burr hole was filled with bone wax. The incision was then closed and the animals were allowed to recover under the care of an animal technician.

Treatment Protocols

Animals with 9L tumors were entered into the imaging study. When *in vivo* tumor volumes reached 20-60 μl, animals were divided into 4 groups. Group one received 0.1 ml of drug vehicle (10% ethanol) and was used as a control group (n=6). Group two (n=4) was treated daily with 10 mg/kg dexamethasone (Dex) which was initiated 3 days prior to the sham BCNU treatment (10% ethanol) and continued for the 7 day imaging study time period. Thus, day 0 for this group had 3 days of Dex treatment prior to baseline imaging. Group three (n=4) received 13.3 mg/kg BCNU diluted in 10% ethanol. Group four (n=3) received the Dex treatment in an identical fashion as Group 2 except that BCNU (13.3 mg/kg) was administered 3 days following initiation of Dex, which was continued daily for the duration of the imaging experiment. All treatments were administered by intraperitoneal injection. Anatomical and diffusion MRI was performed on the day of treatment and repeated on days 3 and 7 post-treatment. In addition FDG-PET imaging was performed two hours before, and at three and seven days post-BCNU.

Diffusion-Weighted MRI

Maps of tumor ADC values were acquired using our previously described method (6). Briefly, a trace diffusion weighted multi-slice spin echo sequence (with motion compensation gradient waveforms and a navigator echo) was used to acquire 13 slices with two different diffusion weightings ($b_1 = 100$ and $b_2 = 1248$ s/mm^2). The b-values represent the sensitivity to diffusion-based contrast in MRI. At least 2 (b-values) are required (b1 and b2) to calculate an apparent diffusion coefficient as described in the ADC equation below. The image slice thickness was 1 mm, image matrix 128×128 (zero filled to 256), field of view 30 × 30 mm and an echo time of 60 ms. During all MRI procedures, animals were anaesthetized using approximately 1.5% isofluorane and body temperature was maintained at 37°C using a heated water re-circulating pad. The images acquired with b_1 were essentially T_2 weighted images and these were used to segment the tumor from normal brain for volumetric analysis using an 'in house' region drawing tool developed in Matlab®.

FDG-PET Imaging

PET imaging of animals was accomplished using either an R4 or P4 micro-PET scanner (Siemens, Knoxville, TN) immediately after each diffusion MRI scan at all time points both preand post-treatment. Once an animal began a study on a particular instrument, that instrument was used for all subsequent time points. Animals were anesthetized with isoflurane and placed on the bed of the instrument and 2-[^{18}F]fluoro-2-deoxy-D-glucose (FDG) (0.9-1.2 mCi) was injected as a bolus via an indwelling tail vein catheter. Animals were fasted for at least 4 hours prior to FDG injection and FDG was allowed to uptake for 40 minutes prior to data acquisition. Six 5-minute images were then acquired serially and images were summed to form a 30 minute average PET image. Images were reconstructed using OSEM (54), 16 subsets, six iterations with Fourier re-binning.

Image Registration and Analysis

Isotropic ADC maps were calculated for each MR image set using the following expression

$$\mathrm{ADC}=\frac{\ln\left(S_1/S_2\right)}{(b_2-b_1)}$$

where S_1 and S_2 are diffusion-weighted images acquired using b_1 and b_2, respectively. ADC pixel value histograms were generated from tumor regions of interest combined across slices. The tumor boundary was manually defined on each slice using a region-of-interest (ROI) tool, and then integrated across slices to determine volume (21). MicroPET images of FDG uptake were then spatially co-registered to their corresponding MR datasets by using a “mutual information for automatic multimodality image fusion” (MIAMI Fuse®) algorithm (55). The ROI masks that were generated to define each tumor volume at each time point were then applied to the corresponding PET dataset and SUV’s were calculated for each tumor at each time point. SUV’s were calculated according to

$$\mathrm{SUV}=\mathrm{FDG}_{\mathrm{region}}/\left(\mathrm{FDG}_{\mathrm{dose}}/\mathrm{WT}\right),$$

where $\mathrm{FDG}_{\mathrm{region}}$ is the decay-corrected regional radiotracer concentration in becquerels per milliliter, $\mathrm{FDG}_{\mathrm{dose}}$ is the injected radiotracer dose in becquerels, and the WT is the body weight in kilograms. All data were analyzed as mean percentage change from pre-treatment values $[(X_{\text{post-Tx}}-X_{\text{pre-Tx}})/X_{\text{pre-Tx}}]$, where X is ADC or SUV. Data are presented as the mean +/− SEM.

Histological Analysis

In a parallel study, sixteen animals with 9L tumors were divided into control, BCNU and BCNU +Dex treatment groups as described above. Anatomical and diffusion MRI was performed on the day of treatment and repeated on days 3 and 7 post-treatment to ensure that the tumors responded similarly to the imaging cohort in terms of diffusion changes over these time intervals. Tissue was removed for control, BCNU and BCNU+Dex treated animals and fixed in buffered formaldehyde for 3 days. Sections were cut on a microtome and paraffin-embedded. H&E staining was accomplished on 8 μm-thick sections for quantification of cells within the tumors. Nuclei were counted in 6 randomly selected fields from sections which provided for quantification of the number of nuclei for each treatment group. Data was quantified as the number of nuclei +/− SEM.

Paraffin sections were deparaffinized in xylene with three changes of 2 min each, then rehydrated through an alcohol gradient of 2 min each (100% alcohol, 90% alcohol, 70%

alcohol, 50% 30%). Antigen retrieval was done by heating the slides in citrate buffer (pH 6.0) for 10 min in a microwave oven. Tissues were then blocked in PBS-T supplemented with 5% normal donkey serum for 1 h. The tissue sections were then incubated with Glut-1 antibody (Abcam, Cambridge, MA) at a dilution of 1:100 and followed by cy3-coupled anti-rabbit secondary antibody (1:200, Jackson Immunoresearch, West Grove, PA). The slides were then counter stained with 1 μg/mL 4′,6-diamidino-2-phenylindole, mounted, and visualized under a fluorescence confocal microscope Nikon Eclipse TE2000-U (Nikon, Melville, NY). In case of MAC-1 staining, CD11b/C antibody coupled to FITC was used at dilation of 1:100. All fluorescence images were acquired using Metamorph software (Molecular Devices Corporation, Sunnyvale, CA) under the same exposure times and images were exported as TIFF files. For quantification of Mac-1 staining the number of MAC-1 positive cells per field were counted. At least two sections per tumor were stained and each group had a minimum of four animals. The Glut-1 stained samples were quantified by calculating the percent area stained which was then normalized for the total number of nuclei per field. Glut-1 staining was quantified in at least two separate fields in every section. There were two sections per animal and a total of four animals per group. The quantitation was performed using Metamorph software (Molecular Devices Corporation, Sunnyvale, CA).

Statistical Methods

Changes in tumor volume, mean FDG uptake and ADC values of the treatment groups were compared at days 3 and 7 using an analysis of variance with a Tukey's multiple comparison statistical test. Differences in cell count, MAC-1 and GLUT-1 between groups were assessed using an unpaired Student's *t*-test. All statistical tests were performed using a statistical software package (SPSS Inc. Chicago, IL) with significance assessed at $p<0.05$.

RESULTS

FDG-PET Treatment Response

PET FDG images were spatially registered to the corresponding MRI data sets. FDG color overlaid images on coronal T2-weighted MR images are shown in Figure 1 which allowed for a more accurate definition of tumor boundaries for prescribing regions-of-interest (ROI) within individual image slices. FDG images of control and Dex-treated (data not shown) animals revealed no major change in FDG uptake over days 3 and 7. Inspection of FDG images of BCNU-treated tumors revealed a noticeable decline in tumor FDG uptake at day 3 post-treatment with a large increase in FDG uptake at day 7 post-treatment (Figure 1). However, treatment of animals with BCNU+Dex showed a drop in FDG uptake at day 3 which persisted at day 7 post-BCNU treatment (Figure 1). Quantification of the average results for all animals was done to provide for statistical comparisons between treatment and time (Figure 1). At three days post-treatment initiation the decrease in mean %SUV observed for both BCNU treated groups (BCNU: $-30.9 \pm 1.2\%$; BCNU+Dex: $-31.4 \pm 9.4\%$) were significantly lower than controls ($4.1 \pm 3.0\%$; $p<0.0001$ and $p<0.0001$, respectively) and Dex treatment ($-3.0 \pm 2.1\%$; $p=002$ and $p=0.003$, respectively). In contrast, no difference was observed between BCNU treated groups. By day 7 BCNU+Dex ($-24.7 \pm 6.5\%$) continued to have a significantly lower mean %SUV than controls ($5.4 \pm 3.7\%$; $p=0.033$). In contrast, animals treated with BCNU alone showed an increase of $20.1 \pm 7.1\%$ from baseline that resulted in a significantly higher mean %SUV than was observed for BCNU+Dex treated animals ($p=0.002$).

Diffusion MRI Treatment Response

Color maps of apparent diffusion values (ADC) for 9L treatment groups (control, BCNU, BCNU+Dex) were overlaid on coronal T2-weighted MR images as shown in Figure 2. Control tumor ADC maps revealed little overall change in the ADC distributions as the tumor increased in size. Images of Dex treated animals revealed very little change in tumor diffusion values

over time (data not shown). Treatment with BCNU resulted in a time-dependent increase in tumor diffusion values as shown in Figure 2 at days 3 and 7 post-treatment. The increase in tumor diffusion values appeared to be fairly spatially uniform throughout the tumor mass over time. To understand the impact of macrophage involvement on influencing ADC changes, results were then compared to those of BCNU+Dex treated tumors (Figure 2). Treatment with the combination of BCNU+Dex also resulted in an increase in tumor ADC values on days 3 and 7. Mean ADC values for each tumor were quantified at days 0, 3 and 7 and the percentage change of ADC from baseline for each group was plotted for days 3 and 7 post-treatment (Figure 2). BCNU treated tumors revealed a time-dependent increase in tumor diffusion values from 10.5 ± 3.2% to 24.4 ± 7.2% at day 3 and day 7 post-treatment, respectively, which were significantly higher than controls (−6.7 ± 1.1%; p=0.008 and p=0.011, respectively)When compared to controls, the BCNU+Dex treated group also exhibited a statistically larger percentage increase in tumor diffusion values on day 3 (11.0 ± 1.1%; p=0.012) as well as on day 7 (21.2 ± 3.1%; p=0.029). Only the BCNU treated group at day 7 was found to be significantly different from Dex treated animals (−1.2 ± 5.7%; p=0.032).

Tumor volumes were assessed using MR images at days 0, 3 and 7 to follow treatment response. As shown in Figure 3, control and Dex animals were found to grow in percent volume from day 0 to day 3 (200 ± 59% and 186 ± 85%, respectively) and day 7 (631 ± 135% and 514 ± 178%, respectively). A reduced percent increase in tumor volume in animals treated with BCNU (70 ± 24% and 198 ± 34% at days 3 and 7, respectively) and BCNU+Dex (38 ± 11% and 86 ± 36% at days 3 and 7, respectively) over control animals was found (Figure 3). No significant difference in percentage change in tumor volume was observed between all groups at day 3 versus day 0. BCNU+Dex was found to have significantly lower percentage change than controls at day 7 (p=0.027) while the BCNU group was found to have a lower tumor volume than control animals (p=0.060).

Quantification of Histology

Evaluation of the impact of treatment-associated responses on the imaging biomarkers was accomplished using H&E, MAC-1 and GLUT-1 for quantification of cell number, macrophage number and the glucose transporter-1 protein, respectively. These studies were undertaken to provide supportive evidence related to the underlying metabolic and cellular changes which occurred following treatment. GLUT-1 was included as GLUT-1 expression is a major reason why tumor cells are FDG positive in PET scans and treatment-dependent changes in expression could impact FDG uptake by the tumor.

Histological analysis of tumor tissue for the untreated and day 7 post-BCNU treatment tumors revealed significant loss of tumor cellularity had occurred (Figure 4A, B). A significant reduction of the number of cell nuclei from 611 ± 40 to 84 ± 10 was observed for the untreated and BCNU-treated tumors, respectively 7 days following BCNU treatment (Figure 4C). The data revealed that BCNU therapy had resulted in a significant therapeutic effect as it resulted in a massive eradication of viable tumor cells within the tumor mass. In order to verify that Dex treatment inhibited the inflammatory response, tumor tissue harvested on day 7 post-treatment was interrogated for the presence of macrophages using MAC-1 staining (Figure 5). Immunofluorescence quantification of the tumor samples revealed that control and BCNU +Dex-treated tumors had small (7.8 ± 1.7) and slightly elevated (20.9 ± 2.4, p<.001) levels of macrophages present, respectively per microscopic field within the tumor tissue. In comparison, BCNU treated tumors were determined to have highly elevated numbers of macrophages (44.7 ± 7.0) per microscopic field which was significantly elevated over control (p<.001) and BCNU+Dex (p<.005) treated tumors (Figure 5). In order to determine if BCNU treatment also produced a decrease in the expression levels of the glucose transporter system in the glioma cells, an immunofluorescent stain for GLUT-1 was used. As shown in Figure 6,

immunofluorescence micrographs of 9L tumor tissue revealed no significant changes ($p>0.05$) in GLUT-1 expression levels could be found between control (0.44 ± 0.04 AFU), BCNU (0.47 ± 0.07 AFU) and BCNU+Dex (0.47 ± 0.06 AFU) treated animals (values are normalized as a percent area stained per number of nuclei).

DISCUSSION

Initial pre-clinical investigations (48) reporting a decrease in FDG uptake hypothesized that a decrease in uptake values is indicative of positive treatment response thus leading to its possible application as a prognostic imaging biomarker of treatment outcome. An early preliminary glioma clinical investigation reported an increase in FDG uptake at day 1 following radiotherapy, which was followed by a decrease in FDG uptake by day 7 (50). The reports of the ability to predict response to therapy based on FDG changes are conflicting with some suggesting that they may correlate with outcome (10,49) while others suggesting they do not (56). Furthermore, [18F]-FDG has been demonstrated to have diagnostic limitations due to the high rate of glucose metabolism in normal brain tissue especially for the detection of low-grade tumors and recurrent high-grade tumors (57,58). However, co-registration of PET images with MRI as done in this study, has been reported to improve the performance of [18F]-PET image interpretation (59). The results presented in this study provide some context to these conflicting reports if consideration is given to the fact that the amount of tumor FDG uptake will not only depend upon the net metabolic rate of the tumor cells themselves, but also on the extent of infiltrating immune cells. Moreover, the temporal interplay of differing populations of cell types and their net impact on the overall %SUV of FDG becomes significantly complex to interpret following successful treatment, as the decline and rise of tumor and inflammatory cell populations may occur at different and unknown rates. In addition, the glucose uptake of the different cell types involved in the dynamic processes associated with a pathophysiological response to therapy may also have varied rates, which would led to an even more complicated scenario for deconvolving the relative contributions of the cell types to their overall contribution to the measured %SUV. The current study was initiated in an effort to better understand the dynamic changes in %SUV for FDG in a tumor treated with chemotherapy as well as the impact and interplay of the effects of the ensuing inflammatory response that occurs in concert with tumor cell death.

Modulation of the immunological response following tumor treatment was accomplished using a corticosteroid, which is used in the management of brain tumor patients for reducing the debilitating effects of brain edema (60). Dexamethasone is known to be effective in suppressing macrophage infiltration, therefore this compound was used to evaluate the effect of modulating immune response on tumor FDG uptake values and diffusion MRI imaging readouts following tumor treatment. As Dex may impact FDG uptake (61-63) and alter tumor ADC values (64), a cohort of Dex-only treated animals were also evaluated and served as an additional “control” arm for interpreting the effects of BCNU+Dex treatment on tumor FDG uptake. Immunohistochemical analysis of tumor specimens revealed that by 7 days post-BCNU treatment, a host therapeutic-associated immune response was induced resulting in a large infiltration of macrophages into the tumor. However, co-treatment with Dex (BCNU+Dex) was found to greatly reduce the influx of immune cells to the tumor at this time point (Figure 5). It was found that baseline levels of tumor FDG uptake (%SUV) were very stable over the 7 day time period for control and Dex-treated animals revealing that Dex produced minimal effect on glucose uptake over this 1 week time period (Figure 1). BCNU treatment resulted in a significant and early decrease in tumor glucose uptake at day 3 post-treatment (−30.9%) compared to controls indicating a significant number of tumor cells were eradicated. This is consistent with a previous report which showed by quantification of histological sections of treated tumors that a significant reduction of 9L tumor cells occurred between 3 and 7 days following BCNU treatment (21) which corresponds with our observed loss in glucose uptake

at day 3. Furthermore, in the current study we observed a dramatic decrease in the percent increase in tumor volume (Figure 3) as well as the approximate 6-fold loss of tumor cells within the tumor mass (Figure 4) as compared to control tumors. These findings reveal that the decrease in tumor FDG uptake at 3 days post-treatment can be attributed to a treatment-induced cell loss which does not recover by day 7. At day 7 a significant reduction in tumor cell density was shown (Figure 4) along with a large net influx of activated macrophages (Figure 5) which corresponded with the observed increase in tumor FDG uptake over baseline levels (Figure 1). These early changes in imaging readouts also correlate with response as BCNU treatment of the 9L tumor resulted in an attenuation of tumor volumes from the time of treatment to days 3 to 7 (Figure 3). Overall, this BCNU dose results in the killing of about 90% of the cells estimated from the significant delay in tumor growth indicating that early changes in tumor imaging biomarkers can be used to predict outcome (20). Moreover, the increased FDG uptake observed on day 7 post-treatment cannot be attributed to tumor regrowth as the tumor cells had not repopulated the mass at this time interval based upon the H&E data (Figure 4) and the increased ADC values (Figure 2). The confirmed presence of a significant inflammatory response within the tumor at day 7 post-treatment corresponds with the increase in FDG uptake (Figure 5) thus is the most likely cell type accounting for increased FDG activity.

Mounting an immune response occurs over time following therapy, which assists in the clearance of macromolecular debris arising from tumor cell death. In this study, we found that following BCNU-treatment, death of 9L glioma cells was accompanied by a large influx of macrophages into the tumor site at day 7 post-treatment. The increase in the number of inflammatory cells within the tumor mass correlated with the observed increase in tumor FDG uptake at day 7 which exceeded that observed prior to therapy by about 20% and was thus significantly higher than FDG uptake levels measured at day 7 post-BCNU therapy in BCNU +Dex treated animals. These results show that the dynamic changes associated with tumor treatment immune response can complicate interpretation of FDG-PET data.

During the course of effective tumor therapy, a reduction in tumor cell density will occur which will reduce the extent of the barriers impeding water diffusion within those regions. The utility of DW-MRI for detecting changes within a tumor following treatment was initially demonstrated using a BCNU treatment of the rat 9L glioma model (19) and was successfully extended in a variety of preclinical studies assessing the response to anticancer interventions (3-6,20,21,[23-29,31,33,35],42,47,52,65). Treatment-induced changes in tumor ADC values have been shown to precede changes in tumor regression, which has provided the rationale for developing this imaging biomarker as an early predictive marker of treatment response. However, the impact of post-treatment immune response on tumor diffusion changes has not been previously evaluated. In this study, we found that Dex administration to 9L animals resulted in negligible alterations in tumor ADC levels versus control animals at up to 7 days (Figure 2). Animals treated with BCNU were found to have a significant increase in tumor diffusion values at day 3 which increased further at day 7 post-treatment as the tumor cells continued to die over time, as demonstrated in previous studies (21). Diffusion values for BCNU+Dex treated animals were not significantly different from BCNU treated animals at days 3 or 7 post-treatment compared with the BCNU only treatment group. This data indicates that a chemotherapy-associated immunological response does not produce a profound effect on the overall detected tumor diffusion response using DW-MRI.

In this study we used the rat 9L glioma model as a system to investigate the impact of the immune response on imaging biomarker readouts of response. Attenuation of the immune response post-therapy provided for a more complete understanding of the impact and temporal nature of macrophage infiltration on DW-MRI and FDG-PET imaging biomarker readouts of treatment response. Both FDG-PET and diffusion MRI detected early changes in the tumor cellular/microenvironment following chemotherapy. Comparison of the effect of the immune

response on the modulation of the two imaging biomarker readouts revealed that by day 7 the effect of BCNU+Dex on ADC measurements were minimal for the BCNU treated animals compared to the observed large increase in tumor FDG uptake. It appears that changes in FDGPET were dramatically affected by the treatment-associated immune response over time to the extent that FDG uptake was higher than pre-treatment levels at day 7 post-BCNU treatment and day 7 values were significantly higher than day 3 values. However, the temporal response profile of DW-MRI was found to be more consistent longitudinally in that although immune modulation was found to be present, the net impact on tumor ADC values was minimal.

In summary, the treatment-associated immune reaction was observed to not significantly impact MR diffusion changes while for FDG-PET scans, it was shown to significantly reverse the initial decline thus complicating the interpretation of FDG-PET for treatment response assessment as an increase in signal may be interpreted as tumor recurrence. Overall, data presented revealed that MRI diffusion measurements were less sensitive to dynamic changes in tumor macrophage content relative to FDG-PET measurements.

STATEMENT OF TRANSLATIONAL RELEVANCE

Imaging biomarkers of cancer treatment response are under active investigation throughout the world. In order to provide clinically prognostic and useful information, changes in imaging biomarker readouts must provide consistent changes reflective of specific underlying alterations in tissue properties including cellular viability, biochemical and molecular responses to therapeutic intervention. Data presented herein show the temporal impact of treatment-associated inflammatory response following chemotherapeutic treatment on FDG-PET and diffusion-weighted MRI imaging readouts. Findings reveal that imaging readouts may be altered significantly by temporal changes associated by the dynamic underlying immunological response to tumor treatment. Interpretation of imaging biomarker readouts of tumor treatment response should take into consideration the potential for changes in cell type subpopulations within the tumor mass over time.

Acknowledgments

Grant support: NIH grants P01CA85878, P50CA93990 and R24CA83099.

REFERENCES

1. Jacobs AH, Kracht LW, Gossmann A, et al. Imaging in neurooncology. NeuroRx 2005;2:333–47. [PubMed: 15897954]
2. Floyd E, McShane TM. Development and use of biomarkers in oncology drug development. Toxicol Pathol 2004;32(Suppl 1):106–15. [PubMed: 15209410]
3. Chenevert TL, Meyer CR, Moffat BA, et al. Diffusion MRI: a new strategy for assessment of cancer therapeutic efficacy. Mol Imaging 2002;1:336–43. [PubMed: 12926229]
4. Chenevert TL, Sundgren PC, Ross BD. Diffusion imaging: insight to cell status and cytoarchitecture. Neuroimaging Clin N Am 2006;16:619–32. viii–ix. [PubMed: 17148023]
5. Hamstra DA, Rehemtulla A, Ross BD. Diffusion magnetic resonance imaging: a biomarker for treatment response in oncology. J Clin Oncol 2007;25:4104–9. [PubMed: 17827460]
6. Moffat BA, Hall DE, Stojanovska J, et al. Diffusion imaging for evaluation of tumor therapies in preclinical animal models. Magma 2004;17:249–59. [PubMed: 15580371]
7. Brock CS, Young H, O'Reilly SM, et al. Early evaluation of tumour metabolic response using [18F] fluorodeoxyglucose and positron emission tomography: a pilot study following the phase II chemotherapy schedule for temozolomide in recurrent high-grade gliomas. Br J Cancer 2000;82:608–15. [PubMed: 10682673]

8. Castell F, Cook GJ. Quantitative techniques in 18FDG PET scanning in oncology. Br J Cancer 2008;98:1597–601. [PubMed: 18475291]
9. Chen W. Clinical applications of PET in brain tumors. J Nucl Med 2007;48:1468–81. [PubMed: 17704239]
10. De Witte O, Hildebrand J, Luxen A, Goldman S. Acute effect of carmustine on glucose metabolism in brain and glioblastoma. Cancer 1994;74:2836–42. [PubMed: 7954245]
11. Franzius C, Schober O. Assessment of therapy response by FDG PET in pediatric patients. Q J Nucl Med 2003;47:41–5. [PubMed: 12714953]
12. Lee JK, Liu RS, Shiang HR, Pan DH. Usefulness of semiquantitative FDG-PET in the prediction of brain tumor treatment response to gamma knife radiosurgery. J Comput Assist Tomogr 2003;27:525–9. [PubMed: 12886136]
13. Pan DH, Guo WY, Chung WY, Shiau CY, Liu RS, Lee LS. Early effects of Gamma Knife surgery on malignant and benign intracranial tumors. Stereotact Funct Neurosurg 1995;64(Suppl 1):19–31. [PubMed: 8584827]
14. Pardo FS, Aronen HJ, Fitzek M, et al. Correlation of FDG-PET interpretation with survival in a cohort of glioma patients. Anticancer Res 2004;24:2359–65. [PubMed: 15330185]
15. Spence AM, Muzi M, Krohn KA. Molecular imaging of regional brain tumor biology. J Cell Biochem Suppl 2002;39:25–35. [PubMed: 12552599]
16. Vlassenko AG, Thiessen B, Beattie BJ, Malkin MG, Blasberg RG. Evaluation of early response to SU101 target-based therapy in patients with recurrent supratentorial malignant gliomas using FDG PET and Gd-DTPA MRI. J Neurooncol 2000;46:249–59. [PubMed: 10902856]
17. Le Bihan D, Breton E, Lallemand D, Aubin ML, Vignaud J, Laval-Jeantet M. Separation of diffusion and perfusion in intravoxel incoherent motion MR imaging. Radiology 1988;168:497–505. [PubMed: 3393671]
18. Szafer A, Zhong J, Gore JC. Theoretical model for water diffusion in tissues. Magn Reson Med 1995;33:697–712. [PubMed: 7596275]
19. Ross BD, Chenevert TL, Kim B, Ben-Joseph O. Magnetic resonance imaging and spectroscopy: Application to experimental neuro-oncology. Q Magn Reson Biol Med 1994;1:89–106.
20. Chenevert TL, McKeever PE, Ross BD. Monitoring early response of experimental brain tumors to therapy using diffusion magnetic resonance imaging. Clin Cancer Res 1997;3:1457–66. [PubMed: 9815831]
21. Chenevert TL, Stegman LD, Taylor JM, et al. Diffusion magnetic resonance imaging: an early surrogate marker of therapeutic efficacy in brain tumors. J Natl Cancer Inst 2000;92:2029–36. [PubMed: 11121466]
22. Chinnaiyan AM, Prasad U, Shankar S, et al. Combined effect of tumor necrosis factor-related apoptosis-inducing ligand and ionizing radiation in breast cancer therapy. Proc Natl Acad Sci U S A 2000;97:1754–9. [PubMed: 10677530]
23. Galons JP, Altbach MI, Paine-Murrieta GD, Taylor CW, Gillies RJ. Early increases in breast tumor xenograft water mobility in response to paclitaxel therapy detected by non-invasive diffusion magnetic resonance imaging. Neoplasia 1999;1:113–7. [PubMed: 10933044]
24. Lee KC, Hall DE, Hoff BA, et al. Dynamic imaging of emerging resistance during cancer therapy. Cancer Res 2006;66:4687–92. [PubMed: 16651420]
25. Lee KC, Hamstra DA, Bhojani MS, Khan AP, Ross BD, Rehemtulla A. Noninvasive molecular imaging sheds light on the synergy between 5-fluorouracil and TRAIL/Apo2L for cancer therapy. Clin Cancer Res 2007;13:1839–46. [PubMed: 17363540]
26. Lee KC, Hamstra DA, Bullarayasamudram S, et al. Fusion of the HSV-1 tegument protein vp22 to cytosine deaminase confers enhanced bystander effect and increased therapeutic benefit. Gene Ther 2006;13:127–37. [PubMed: 16163381]
27. Lee KC, Moffat BA, Schott AF, et al. Prospective early response imaging biomarker for neoadjuvant breast cancer chemotherapy. Clin Cancer Res 2007;13:443–50. [PubMed: 17255264]
28. Lee KC, Sud S, Meyer CR, et al. An imaging biomarker of early treatment response in prostate cancer that has metastasized to the bone. Cancer Res 2007;67:3524–8. [PubMed: 17440058]
29. Moffat BA, Chenevert TL, Meyer CR, et al. The functional diffusion map: an imaging biomarker for the early prediction of cancer treatment outcome. Neoplasia 2006;8:259–67. [PubMed: 16756718]

30. Poptani H, Puumalainen AM, Grohn OH, et al. Monitoring thymidine kinase and ganciclovir-induced changes in rat malignant glioma in vivo by nuclear magnetic resonance imaging. Cancer Gene Ther 1998;5:101–9. [PubMed: 9570301]

31. Ross BD, Moffat BA, Lawrence TS, et al. Evaluation of cancer therapy using diffusion magnetic resonance imaging. Mol Cancer Ther 2003;2:581–7. [PubMed: 12813138]

32. Schepkin VD, Lee KC, Kuszpit K, et al. Proton and sodium MRI assessment of emerging tumor chemotherapeutic resistance. NMR Biomed 2006;19:1035–42. [PubMed: 16894643]

33. Stegman LD, Rehemtulla A, Hamstra DA, et al. Diffusion MRI detects early events in the response of a glioma model to the yeast cytosine deaminase gene therapy strategy. Gene Ther 2000;7:1005–10. [PubMed: 10871748]

34. Zhao M, Pipe JG, Bonnett J, Evelhoch JL. Early detection of treatment response by diffusion-weighted 1H-NMR spectroscopy in a murine tumour in vivo. Br J Cancer 1996;73:61–4. [PubMed: 8554985]

35. Hamstra DA, Chenevert TL, Moffat BA, et al. Evaluation of the functional diffusion map as an early biomarker of time-to-progression and overall survival in high-grade glioma. Proc Natl Acad Sci U S A 2005;102:16759–64. [PubMed: 16267128]

36. Hayashida Y, Yakushiji T, Awai K, et al. Monitoring therapeutic responses of primary bone tumors by diffusion-weighted image: Initial results. Eur Radiol 2006;16:2637–43. [PubMed: 16909220]

37. Hein PA, Kremser C, Judmaier W, et al. Diffusion-weighted magnetic resonance imaging for monitoring diffusion changes in rectal carcinoma during combined, preoperative chemoradiation: preliminary results of a prospective study. Eur J Radiol 2003;45:214–22. [PubMed: 12595106]

38. Kamel IR, Bluemke DA, Eng J, et al. The role of functional MR imaging in the assessment of tumor response after chemoembolization in patients with hepatocellular carcinoma. J Vasc Interv Radiol 2006;17:505–12. [PubMed: 16567675]

39. Kremser C, Judmaier W, Hein P, Griebel J, Lukas P, de Vries A. Preliminary results on the influence of chemoradiation on apparent diffusion coefficients of primary rectal carcinoma measured by magnetic resonance imaging. Strahlenther Onkol 2003;179:641–9. [PubMed: 14628131]

40. Mardor Y, Pfeffer R, Spiegelmann R, et al. Early detection of response to radiation therapy in patients with brain malignancies using conventional and high b-value diffusion-weighted magnetic resonance imaging. J Clin Oncol 2003;21:1094–100. [PubMed: 12637476]

41. Mardor Y, Roth Y, Lidar Z, et al. Monitoring response to convection-enhanced taxol delivery in brain tumor patients using diffusion-weighted magnetic resonance imaging. Cancer Res 2001;61:4971–3. [PubMed: 11431326]

42. Moffat BA, Chenevert TL, Lawrence TS, et al. Functional diffusion map: a noninvasive MRI biomarker for early stratification of clinical brain tumor response. Proc Natl Acad Sci U S A 2005;102:5524–9. [PubMed: 15805192]

43. Pickles MD, Gibbs P, Lowry M, Turnbull LW. Diffusion changes precede size reduction in neoadjuvant treatment of breast cancer. Magn Reson Imaging 2006;24:843–7. [PubMed: 16916701]

44. Roth Y, Tichler T, Kostenich G, et al. High-b-value diffusion-weighted MR imaging for pretreatment prediction and early monitoring of tumor response to therapy in mice. Radiology 2004;232:685–92. [PubMed: 15215551]

45. Theilmann RJ, Borders R, Trouard TP, et al. Changes in water mobility measured by diffusion MRI predict response of metastatic breast cancer to chemotherapy. Neoplasia 2004;6:831–7. [PubMed: 15720810]

46. Tomura N, Narita K, Izumi J, et al. Diffusion changes in a tumor and peritumoral tissue after stereotactic irradiation for brain tumors: possible prediction of treatment response. J Comput Assist Tomogr 2006;30:496–500. [PubMed: 16778628]

47. Hamstra DA, Galban CJ, Meyer CR, et al. Functional diffusion map as an early imaging biomarker for high-grade glioma: correlation with conventional radiologic response and overall survival. J Clin Oncol 2008;26:3387–94. [PubMed: 18541899]

48. Abe Y, Matsuzawa T, Fujiwara T, et al. Assessment of radiotherapeutic effects on experimental tumors using 18F-2-fluoro-2-deoxy-D-glucose. Eur J Nucl Med 1986;12:325–8. [PubMed: 3792361]

49. Rozental JM, Cohen JD, Mehta MP, Levine RL, Hanson JM, Nickles RJ. Acute changes in glucose uptake after treatment: the effects of carmustine (BCNU) on human glioblastoma multiforme. J Neurooncol 1993;15:57–66. [PubMed: 8384254]

50. Rozental JM, Levine RL, Mehta MP, et al. Early changes in tumor metabolism after treatment: the effects of stereotactic radiotherapy. Int J Radiat Oncol Biol Phys 1991;20:1053–60. [PubMed: 2022505]
51. Andersen PB, Blinkenberg M, Lassen U, et al. A prospective PET study of patients with glioblastoma multiforme. Acta Neurol Scand 2006;113:412–8. [PubMed: 16674608]
52. Ross DA, Sandler HM, Balter JM, Hayman JA, Archer PG, Auer DL. Imaging changes after stereotactic radiosurgery of primary and secondary malignant brain tumors. J Neurooncol 2002;56:175–81. [PubMed: 11995819]
53. Waarde AV, Cobben DCP, Suurmeijer AJH, Maas B, Vaalburg W, de Vries EFJ, Jager PL, Hoekstra HJ, Elsinga PH. Selectivity of 18F-FLT and 18F-FDG for differentiating tumor from inflammation in a rodent model. J. Nucl. Med 2004;45:695–700. [PubMed: 15073267]
54. Yao R, Seidel J, Johnson CA, Daube-Witherspoon ME, Green MV, Carson RE. Performance characteristics of the 3-D OSEM algorithm in the reconstruction of small animal PET images. Ordered-subsets expectation-maximixation. IEEE Trans Med Imaging 2000;19:798–804. [PubMed: 11055803]
55. Kim B, Boes JL, Frey KA, Meyer CR. Mutual information for automated unwarping of rat brain autoradiographs. Neuroimage 1997;5:31–40. [PubMed: 9038282]
56. Janus TJ, Kim EE, Tilbury R, Bruner JM, Yung WK. Use of [18F]fluorodeoxyglucose positron emission tomography in patients with primary malignant brain tumors. Ann Neurol 1993;33:540–8. [PubMed: 8498831]
57. Olivero WC, Dulebohn SC, Lister JR. The use of PET in evaluating patients with primary brain tumors: is it useful? J Neurol Neurosurg Psychiatry 1995;58:250–52. [PubMed: 7876865]
58. Ricci PE, Karis JP, Heiserman JE, Fram EK, Bice AN, Drayer BP. Differentiating recurrent tumor from radiation necrosis: time for re-evaluation of positron emission tomography? Am J Neuroradiol 1998;19:407–413. [PubMed: 9541290]
59. Wong TZ, Turkington TG, Hawk TC, Coleman RE. PET and brain tumor image fusion. Cancer J 2004;10:234–242. [PubMed: 15383204]
60. Kaal EC, Vecht CJ. The management of brain edema in brain tumors. Curr Opin Oncol 2004;16:593–600. [PubMed: 15627023]
61. Fulham MJ, Brunetti A, Aloj L, Raman R, Dwyer AJ, Di Chiro G. Decreased cerebral glucose metabolism in patients with brain tumors: an effect of corticosteroids. J Neurosurg 1995;83:657–64. [PubMed: 7674016]
62. Mamede M, Saga T, Ishimori T, et al. Differential uptake of (18)F-fluorodeoxyglucose by experimental tumors xenografted into immunocompetent and immunodeficient mice and the effect of immunomodification. Neoplasia 2003;5:179–83. [PubMed: 12659691]
63. Roelcke U, Blasberg RG, von Ammon K, et al. Dexamethasone treatment and plasma glucose levels: relevance for fluorine-18-fluorodeoxyglucose uptake measurements in gliomas. J Nucl Med 1998;39:879–84. [PubMed: 9591593]
64. Bastin ME, Carpenter TK, Armitage PA, Sinha S, Wardlaw JM, Whittle IR. Effects of dexamethasone on cerebral perfusion and water diffusion in patients with high-grade glioma. AJNR Am J Neuroradiol 2006;27:402–8. [PubMed: 16484419]
65. Hamstra DA, Lee KC, Tychewicz JM, et al. The use of 19F spectroscopy and diffusion-weighted MRI to evaluate differences in gene-dependent enzyme prodrug therapies. Mol Ther 2004;10:916–28. [PubMed: 15509509]

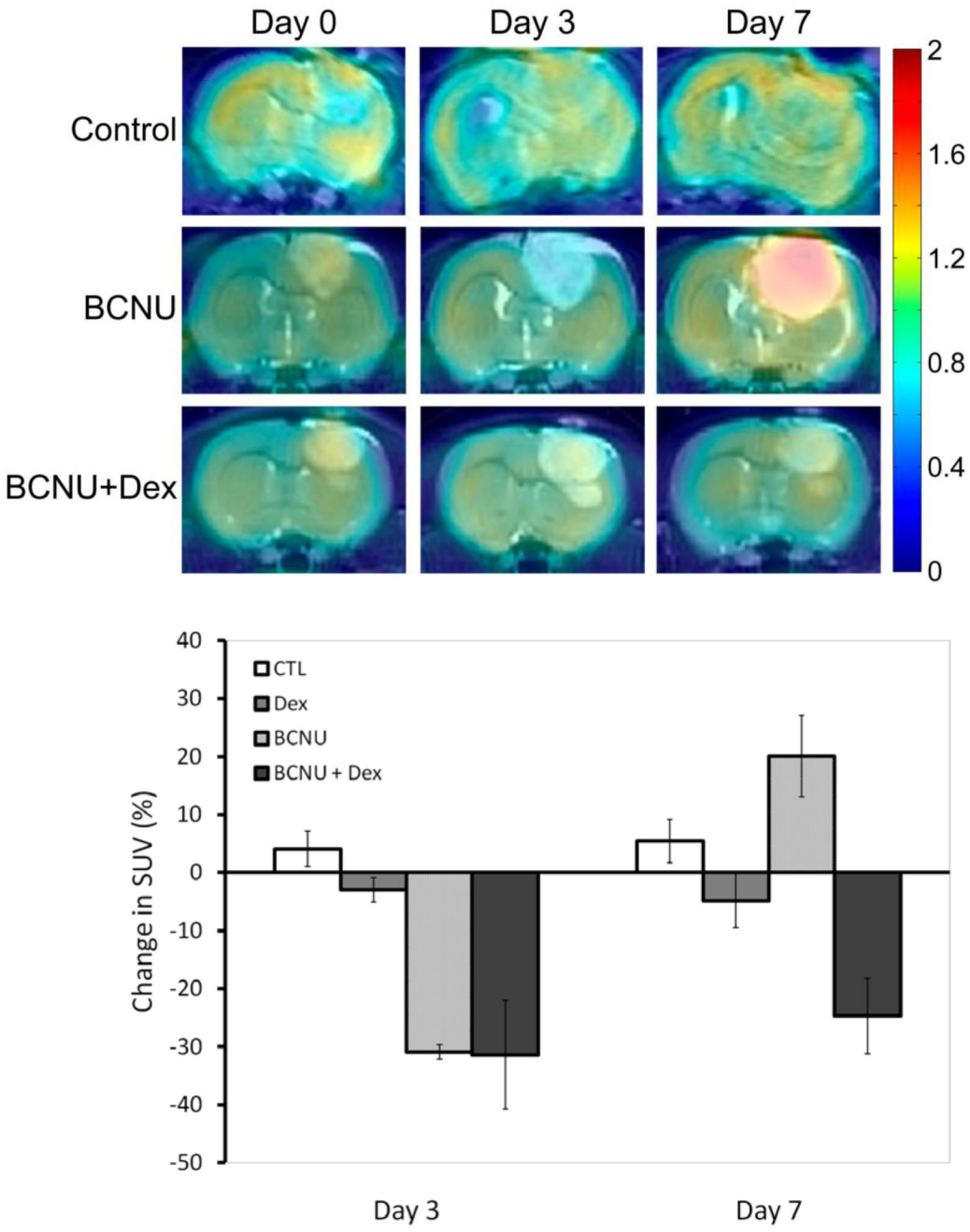

Figure 1. Coregistered FDG-PET and MR images

Coronal images of FDG tumor uptake (color overlay) registered with T2-weighted MR images for a control, BCNU treated, and a BCNU + Dex treated animal over time at pre-treatment (day 0) and repeated on days 3 and 7 post-treatment. Color scale represents the fold-increase over normal contralateral brain tissue. **Change in FDG-PET.** Percentage change in FDG tumor uptake for control, Dex, BCNU and BCNU + Dex treated animals at day 3 and 7 post-treatment.

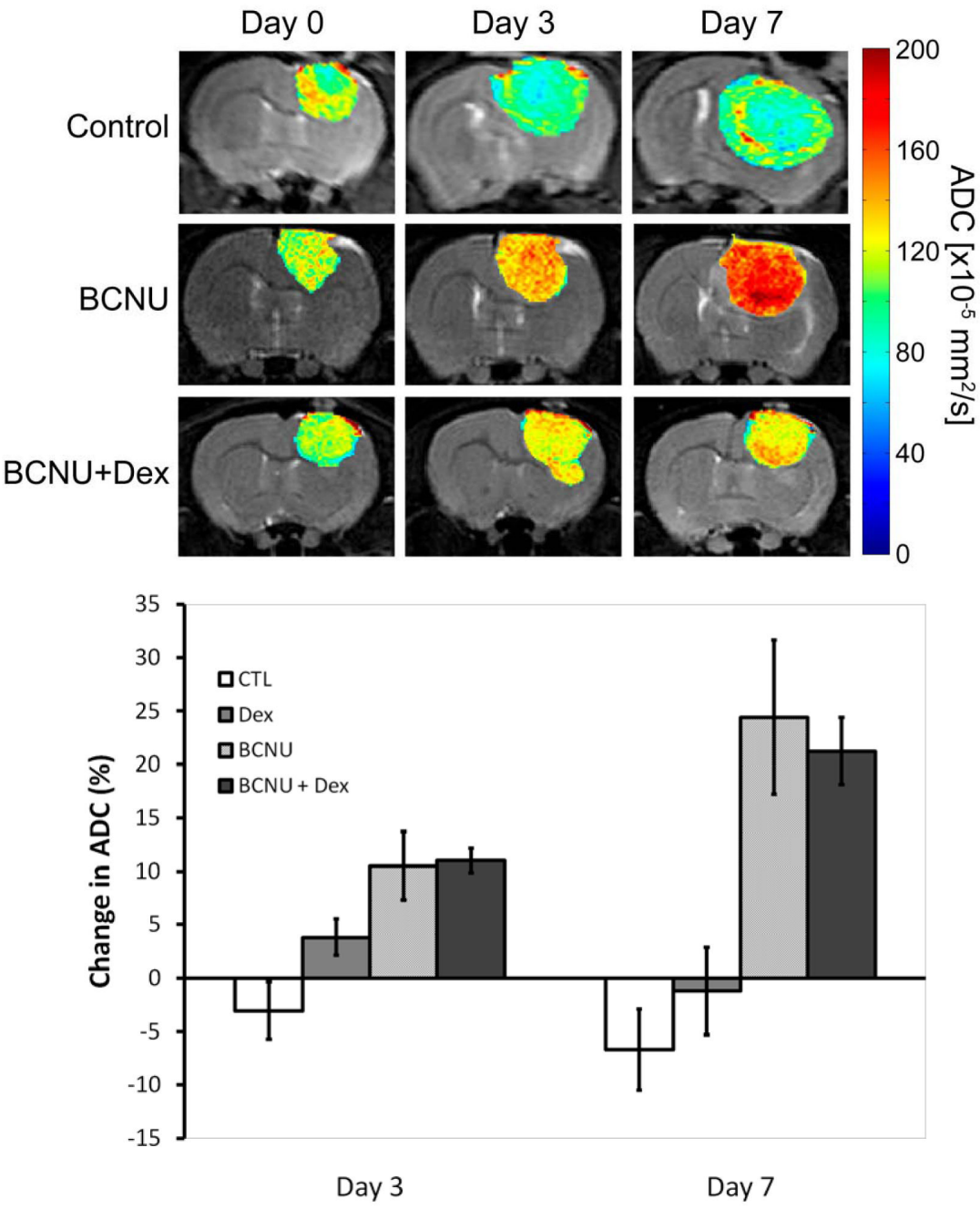

Figure 2. Diffusion MRI

Representative coronal images of intracerebreal 9L tumors ADC ($x10^{-11}m^2/s$) maps shown as color overlays on registered T2-weighted MR images of a control, BCNU and BCNU + Dex treated animal over time at pre-treatment (day 0) and repeated on days 3 and 7 post-treatment. **Change in ADC.** Percentage change in tumor ADC for control, Dex, BCNU, and BCNU + Dex treated animals at days 3 and 7 post-treatment.

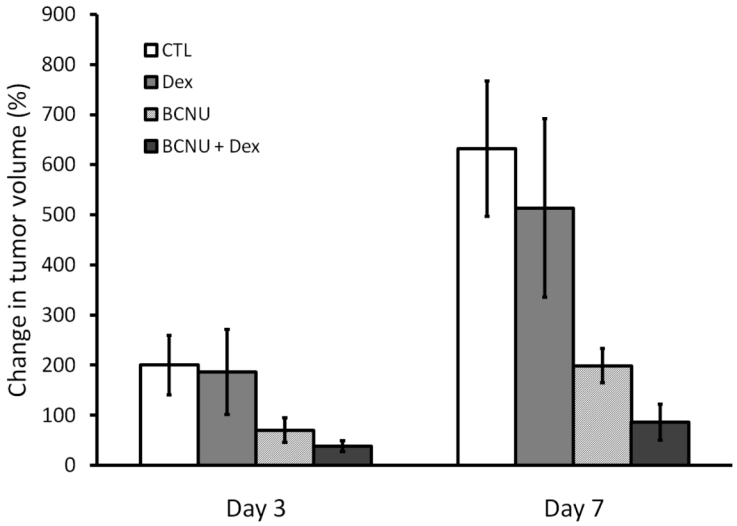

Figure 3. Change in tumor volume

The mean percentage change in intracerebral 9L tumor volumes determined from T2-weighted MR images are shown for control, Dex, BCNU, and BCNU + Dex treated animals at days 3 and 7 post-treatment.

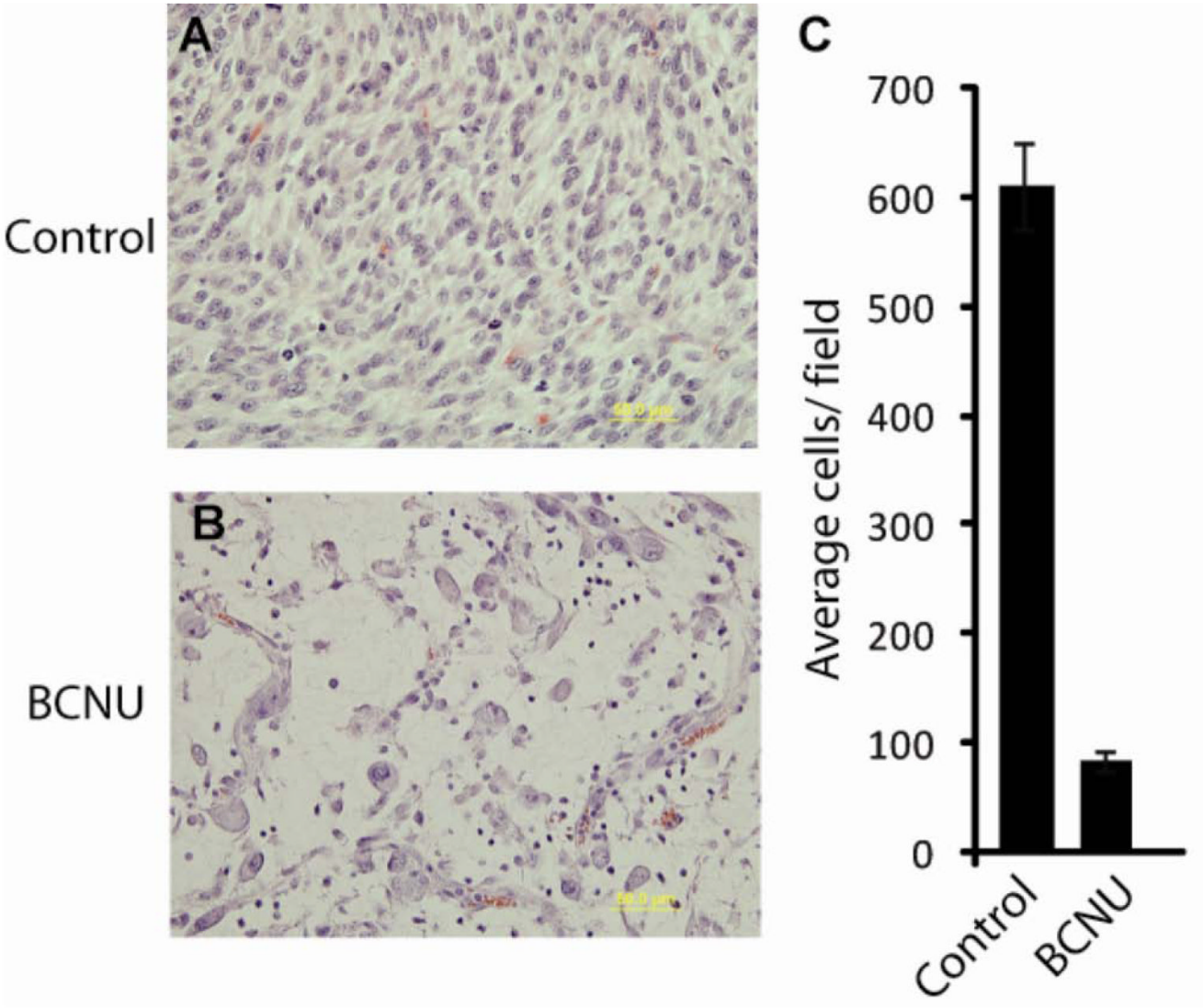

Figure 4. Morphologic analysis

(A) Control or (B) BCNU treated tumors were stained with H and E and nuclei were counted in randomly selected fields. Representative micrographs for each group is shown. (C) Bar graph depicts the quantification of the nuclei for each treatment group in 6 randomly selected fields. Data represented is number of nuclei +/− SEM.

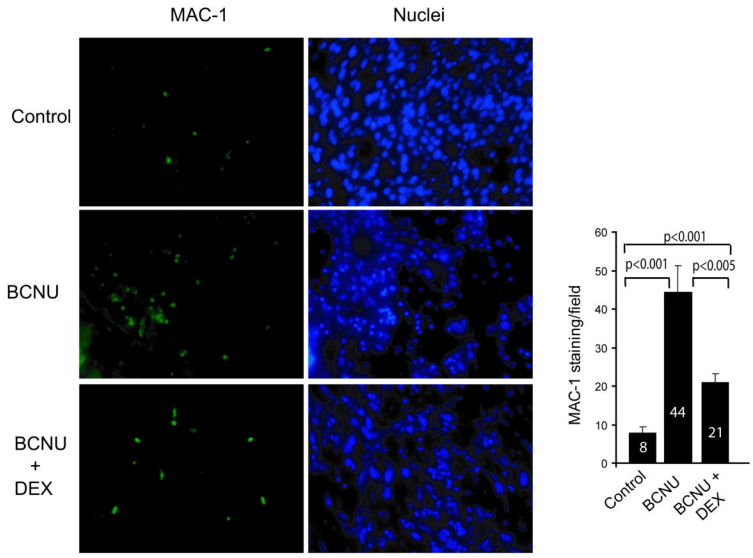

Figure 5. MAC-1 staining in tumor micrographs

Immunofluorescence staining of control, BCNU treated and BCNU plus dexamethasone treated tumors was performed using on MAC-1 antibody. A representative immunofluorescence micrograph for each group is shown. The number of cells positive for Mac-1 signal within tumor were counted per field. At least two sections per tumor were stained. Each group had a minimum of four animals. The Students *t*-test showed that the difference between the control and BCNU, control and BCNU+DEX or BCNU and BCNU+DEX was significant for the MAC-1 positive cells.

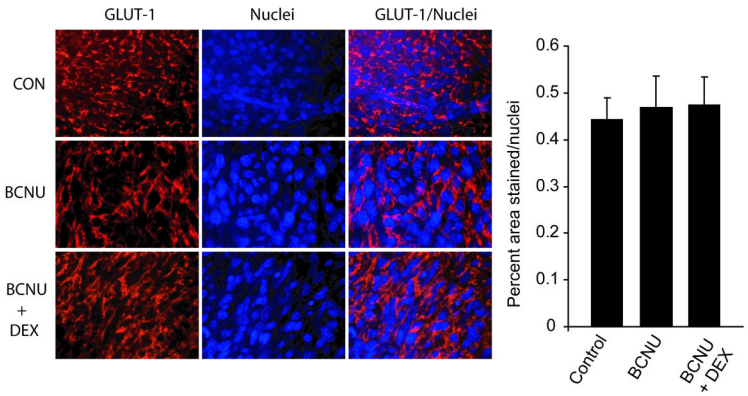

Figure 6. GLUT-1 staining in tumor micrographs

Immunofluorescence staining of control, BCNU treated and BCNU and Dexamethasone treated tumors was performed using a GLUT-1 antibody. A representative immunofluorescence micrograph for each group is shown. Bar graph depicts the quantification of the results for each treatment group from four animals per group with at least 2 sections per animal and 2 fields per section.